www.czasopisma.pan.pl PAN POLSKA AKADEMIA NAUK www.journals.pan.pl

Arch. Min. Sci. **64** (2019), 4, 671-686

Electronic version (in color) of this paper is available: http://mining.archives.pl

DOI 10.24425/ams.2019.129376

ZHENQI LIU*, XIAOXING ZHONG**#, BOTAO QIN*,
HONGWEI REN*, ANG GAO*

REDEVELOPMENT OF FRACTURES AND PERMEABILITY CHANGES AFTER MULTI-SEAM MINING OF SHALLOW CLOSELY SPACED COAL SEAMS

POWSTAWANIE SPĘKAŃ WTÓRNYCH I ZMIANY PRZEPUSZCZALNOŚCI SKAŁ WSKUTEK EKSPLOATACJI WIELO-POKŁADOWEJ ZŁÓŻ WĘGLA W PŁYTKICH I BLISKO ZALEGAJĄCYCH POKŁADACH

Mining the lower seams in a sequence of shallow, closely spaced coal seams causes serious air leakage in the upper goaf; this can easily aggravate spontaneous combustion in abandoned coal. Understanding the redevelopment of fractures and the changes in permeability is of great significance for controlling coal spontaneous combustion in the upper goaf. Based on actual conditions at the 22307 working face in the Bulianta coal mine, Particle Flow Code (PFC) and a corresponding physical experiment were used to study the redevelopment of fractures and changes in permeability during lower coal seam mining. The results show that after mining the lower coal seam, the upper and lower goafs become connected and form a new composite goaf. The permeability and the number of fractures in each area of the overlying strata show a pattern of „stability-rapid increase-stability" as the lower coal seam is mined and the working face advances. Above the central area of goaf, the permeability has changed slightly, while in the open-cut and stop line areas are significant, which formed the main air leakage passage in the composite goaf.

Keywords: shallow closely spaced coal seams; multi-seam mining; fracture redevelopment; permeability changes

Wybieranie kolejnych płytkich sąsiadujących ze sobą pokładów w ramach eksploatacji złóż węgla prowadzi do znaczących wypływów powietrza w zrobach leżących powyżej, co spowodować może wzrost zagrożenia pożarowego wskutek samo-zapłonu węgla pozostałego w zrobach.

Dokładne zrozumienie zjawiska powstawania wtórnych spękań skał oraz zmian w ich przepuszczalności ma podstawowe znaczenie dla skutecznego zapobiegania samo-zapłonom węgla w zrobach zalegających powyżej pokładów wybieranych. W oparciu o dane dotyczące aktualnych warunków

* KEY LABORATORY OF GAS AND FIRE CONTROL FOR COAL MINES (CHINA UNIVERSITY OF MINING AND TECHNOLOGY), MINISTRY OF EDUCATION, XUZHOU, 221116, CHINA

** SCHOOL OF SAFETY ENGINEERING, CHINA UNIVERSITY OF MINING AND TECHNOLOGY, XUZHOU 221116, CHINA

Corresponding author: zhxxcumt@163.com

panujących w rejonie ściany nr 22307 w kopalni węgla Bulianta i wykorzystując oprogramowanie Particle Flow Code (PFC) a także wyniki odpowiednich eksperymentów fizycznych, przeanalizowano procesy powstawania wtórnych spękań skał i zmian ich przepuszczalności w trakcie wybierania niżej zalęgających pokładów wskutek połączenia zrobów leżących na różnych poziomach i powstania nowego, połączonego obszaru zrobów. Przepuszczalność i ilość spękań w każdym obszarze warstw nadkładu kształtuje się według schematu: 'stabilność-gwałtowny wzrost-stabilność' w miarę postępu przodka i postępowania prac w niżej zalegającym pokładzie. W warstwach nadkładu leżących bezpośrednio ponad środkową częścią zrobów obserwuje się nieznaczne zmiany przepuszczalności, podczas gdy w obszarach wybierania i w obszarach gdzie wybieranie się zakończyło zmiany przepuszczalności będą znaczne, prowadząc do powstania głównego korytarza wypływu powietrza w nowo-powstałym, połączonym obszarze zrobów.

Słowa kluczowe: płytkie i blisko zalegające pokłady węgla, eksploatacja wielo-pokładowa, powstawanie spękań wtórnych, zmiany przepuszczalności

1. Introduction

Western China is rich in coal resources. The major coalfields are relatively shallow with multiple closely spaced seams under thin bedrock roofs, for example the Shendong and Northern Shanxi (Li Tao et al., 2011) fields. These characteristics are favorable for mining, but these coals are also prone to spontaneous combustion. In many mines, the first main coal seam has been or is about to be mined and mining of the second main coal seam has started. When the lower coal seam in a sequence of shallow and closely spaced coal seams is mined, the overlying strata and the upper goaf are disturbed twice. This leads to the reactivation of fractures and the development of new fractures and this increases atmospheric air leakage into the goaf. This makes spontaneous combustion more likely. Spontaneously combusting coal in these coalfields is fairly common and it has greatly affected safe and efficient mining as well as resulting in huge economic losses and serious social impacts (Zhang Xiaomei, 2012). Understanding the mining-induced fracture patterns in the strata overlying shallow closely spaced coal seams can be beneficial for preventing or controlling spontaneous combustion fires in the goaf after those seams are mined.

Concerning the development of fractures after shallow coal seam mining, M. Cymbarerich (1957) put forward the step sinking theory for shallow coal seam mining. He proposed that where the coal bed was shallow, the overlying strata could be regarded as a homogeneous body whose roof was cut along the coal wall to the ground surface by an inclined hexahedron as the working face advanced. In another study, Buizen (1991) found that the strata along the working face and the edge of the goaf were fractured almost vertically as the working face advanced. Holla (2012) concluded that during shallow coal seam mining, the roof collapse height was nine times the height of the mining height and the roof broke quickly after the working face advanced. Shallow coal seam mining practice in India has shown that the caving zone in the overlying strata intersects the fractures zone, the fractures zone is quite high, and the fracture network is dense (Singh and Yadav, 1995; JIANG Fuxing et al., 2002). Fan Gangwei (et al., 2011) studied a coal bed in the Shendong mining area in China and used a laboratory-scale physical model of the mine and numerical simulations to analyze changes in movement in the overlying strata and the distribution and expansion of fractures after longwall mining of shallow coal seams. The physical model is used by Tu Hong-Sheng (et al., 2017) to analyze the change characteristics of the overlying strata fissure and stability along with the mining face. The results show that the model coincides very well with the site conditions. Hua Guo (et al., 2012) monitored the

changes in overlying strata subsidence, stress, and water pressure during mining in the Guqiao coal mine in China and used numerical simulations to investigate collapse of the overlying strata. The above studies all investigated localities where only a single coal seam was mined. Investigations concerning the mining of multiple, closely spaced seams include a study by Cheng Zhiheng (et al., 2016) who used experiments to study dynamic stresses and fracture dynamics during mining of closely spaced coal seams. Ma Haifeng (et al., 2017) determined how mining stress evolved and characterized the displacement field in the overlying strata during mining of closely spaced seams using simulations and engineering practice. Zhao Tuanzhi (et al., 2009) used numerical simulation to simulate the advancing stress field and the dynamic development of the separated layer in a working face. Zhu Weibing (2011) made a detailed study of strata instability and rock pressure in shallow, closely spaced coal seams in the Shendong mining area in China. Chu Tingxiang (et al., 2010) concluded that the mechanical properties of the rock between the upper and lower coal seams significantly influenced the height of the caving zone and the rock fractures. In a study aimed at long wall mining of closely spaced coal seams under shallow buried goaf in the Shendong coalfield. Wang Fangtian (2012) completed a systematic analysis of the stability of coal pillars and the prevention of and remediation methods for roof pressures over large areas. That study also considered movement in the strata overlying closely spaced coal seams and strategies to control roof movement when mining under goaf. Ma Liqiang (et al., 2013; et al., 2015) used physical simulation experiments to study deformation and fracture development in strata overlying an area that had been repeatedly disturbed by the mining of shallow and closely spaced coal seams. Hu Chenglin (2014) employed numerical simulations to investigate the temporal and spatial changes in water-conducting fractures in shallow and closely spaced coal seams before and after repeated cycles of mining in the Shendong Shigetai mine in China. Jin Zhiyuan (2015) carried out systematic analysis on mechanisms that control water transmission fractures in the strata overlying shallow, closely spaced coal seams. Xue Dongjie (et al., 2015) revealed how mining fractures evolve based on geological conditions in the Daliuta Mine in China and evaluated the evolution of mining fractures quantitatively using fractals and percolation theory. Tian-Rang, Jia (et al., 2013) used the RFPA-Gas software to study the fracture characteristics of overlying strata during the mining of the cover. Wen Hu (et al., 2015) used physical simulation experiments and numerical analysis to analyze the temporal and spatial evolution law of fractures and stress distribution in the overlying strata during the mining of upper and lower coal seams.

At present, the study of closely spaced coal seams mainly revolves around lithostatic pressure, overlying strata displacement, and the study of water-conducting fractures. There have been no systematic studies on air leakage from fissures or permeability during mining. This paper investigates the changes in the permeability and fractures in the strata overlying shallow, closely spaced coal seams during mining and analyzes how the subsequent mining of a seam below a previously mined seam affects the permeability and redistributes the fractures in the overlying strata.

2. Working faces in the Bulianta coal mine

The No. 22307 face in the Bulianta coal mine, Inner Mongolia, China, is located in the third area of the No. 22 coal seam in the second main coal seam , the buried depth is about 130 m. The overlying goaf is from a mined-out portion of the first main coal seam, the No. 12 coal 12308

working face. The average distance between the two seams is 39 m and the seams dip at 1°-3°. The average coal thickness at the 12308 face is 5.91 m, the design mining height is 3.5 m, and the average daily advance is 10.4 m. The average coal thickness at the 22307 face is 7.25 m, the design mining height is 6.8 m, and the average daily advance is 17 m. At these working faces, the first collapsing interval for both seam faces is generally about 50 m and the periodic collapsing interval is around 10-15 m. Figure 1 is a diagrammatic cross section showing the stratigraphy and the two working faces. Table 1 lists the macroscopic mechanical properties of strata shown in 1.

TABLE 1

Macroscopic mechanical properties for the sedimentary units shown in Fig. 1

Stratum number	Lithology	Bulk Density (kg/m^3)	Poisson ratio	Modulus of elasticity /GPa	Tension strength /MPa	Compression strength/MPa	Cohesion /MPa	Internal friction angle/°
1	Aeolian Sand	1580	0.2	12.2	0.82	11.61	0.54	33.48
2	Siltstone	2650	0.18	19.4	2.28	29.80	4.12	36.4
3	Medium Sandstone	2250	0.17	33.4	8.82	22.98	7.12	35.30
4	Coal	1290	0.29	12.6	1.18	17.51	2.27	32.42
5	Sandy Mudstone	2410	0.18	25.3	1.48	45.98	4.12	34.48
6	Sandy Mudstone	2370	0.19	23.2	2.28	29.80	4.12	34.48
7	Sandy Mudstone	2410	0.18	25.3	1.48	45.98	4.12	34.48
8	Coal	1240	0.29	12.6	1.12	18.45	2.27	32.42
9	Sandy Mudstone	2370	0.19	23.2	2.28	29.80	4.12	34.48

3. Numerical and physical models

3.1. Determination of mesoscopic parameters

The numerical model in this paper was solved with the help of PFC code, so the proper selection of meso-mechanical parameters is the key to simulation using PFC. There are two types of mesoscopic parameters was determined in PFC, the deformability and strength parameters. Scholars conducted a large number of uniaxial compression and Brazilian splitting tests and numerical simulation during the relevant researches, established the empirical formulas between the macroscopic and mesoscopic parameters (Wang Tao et al., 2014). The deformability parameters include the meso-Young's modulus (*Ec*) and the ratio of normal stiffness to shear stiffness (k_n/k_s), and the formulae are shown in Eqs. (1) and (2).

$$E / E_c = a + b \ln(k_n / k_s) \tag{1}$$

$$v = c \ln(k_n / k_s) + d \tag{2}$$

where E is macro-elastic modulus; GPa, Ec is Young's modulus; GPa, v is Poisson's ratio, k_n/k_s represent the normal-to-shear stiffness ratio, k_n is normal stiffness; MPa, k_s is shear stiffness; MPa, $a = 1.652$, $b = -0.395$, $c = 0.209$, $d = 0.111$.

The mesoscopic strength parameters include the normal strength of parallel bond ($\bar{\sigma}$) and shear strength of parallel bond ($\bar{\tau}$),the regression formulae are shown in Eqs. (3) and (4).

$$\frac{\sigma_c}{\bar{\sigma}} = \begin{cases} a\left(\frac{\bar{\tau}}{\bar{\sigma}}\right)^2 + b\frac{\bar{\tau}}{\bar{\sigma}}, & 0 < \frac{\bar{\tau}}{\bar{\sigma}} \le 1 \\ c, & \frac{\bar{\tau}}{\bar{\sigma}} \ge 1 \end{cases} \tag{3}$$

$$\frac{\sigma_t}{\bar{\sigma}} = \begin{cases} d\left(\frac{\bar{\tau}}{\bar{\sigma}}\right)^2 + e\frac{\bar{\tau}}{\bar{\sigma}}, & 0 < \frac{\bar{\tau}}{\bar{\sigma}} \le 1 \\ f, & \frac{\bar{\tau}}{\bar{\sigma}} \ge 1 \end{cases} \tag{4}$$

where σ_t is tensile strength; MPa, σ_c is uniaxial compressive strength; MPa, $a = -0.965$, $b = 2.292$, $c = 1.327$, $d = -0.174$, $e = 0.463$, and $f = 0.289$.

In this work, the initial value of the meso-mechanical parameters is determined according to the empirical formulas. These values were fine-tuned repeatedly and taken as references to perform corresponding numerical tests. The final meso-mechanical parameters were determined by repeating this process until the obtained macro-mechanical parameters and the required values are consistent. The mesoscopic properties for the different rock units used in the numerical simulation are shown in Table 2.

TABLE 2

Mesoscopic properties parameters for sedimentary units used in the numerical model

Stratum number	Lithology	ρ /kg·m^{-3}	*Ks* /GPa	*Kn* /GPa	*Pb_Kn* /GPa	*Pb_Ks* /GPa	*Pb_ten* /Pa	*Pb_coh* /Pa
1	Aeolian Sand	1975	7.33	10.23	12.4	9.48	5×10^5	1×10^6
2	Siltstone	2963	14.88	21.74	25.11	16.52	1.7×10^6	4.3×10^7
3	Medium Sandstone	2813	18.62	24.71	9.4	7.27	1.6×10^6	2.1×10^7
4	Coal	1550	3.83	9.25	5.2	2.77	1×10^7	1×10^7
5	Sandy Mudstone	3013	16.2	22.32	16.94	10.67	1.7×10^6	5×10^7
6	Sandy Mudstone	2963	14.35	20.6	24.43	16.13	1.7×10^6	4.3×10^7
7	Sandy Mudstone	3013	16.2	22.32	16.94	10.67	1.7×10^6	5×10^7
8	Coal	1550	3.83	9.25	5.2	2.77	1×10^7	1×10^7
9	Sandy Mudstone	2963	14.35	22.32	16.94	10.67	1.7×10^6	4.3×10^7

Ks: Shear stiffness; *Kn*: Normal stiffness; *Pb_Kn*: Normal stiffness of parallel bond; *Pb_Ks*: Shear stiffness of parallel bond; *Pb_ten*: Parallel bond strength; *Pb_coh*: *cohesion.*

3.2. Numerical model

The numerical model has dimensions identical to those of the actual Bulianta coal mine, the numerical model is constructed at a 1:1 ratio to the dimensions shown in Fig. 1. The model length is 300 m, the height is 140 m, and the model is divided into nine horizontal layers. The models' left and right boundary walls are fixed to limit horizontal displacement, the bottom boundary is

fixed to limit vertical displacement, and the top is a free boundary. In order to eliminate boundary effects, a 15 m protective coal pillar is reserved on the left side of the upper coal seam and a 25 m pillar is reserved on the right side. The alternate interior length on the left side of the lower coal seam to the left side of the upper coal seam is 10 m; the alternate exterior length on the right side of the lower coal seam to upper coal seam is 10 m.

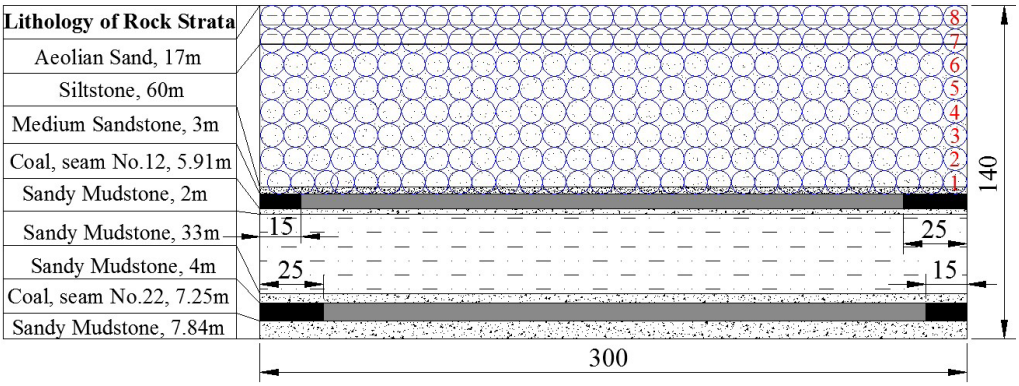

Fig. 1. Diagrammatic cross section showing the stratigraphic section in a portion of the Bulianta coal mine. The dimensions are those used in the numerical and physical models described in the next section of this paper. The eight rows of circles in the figure above the No. 12 coal are "measuring circles;" see text for an explanation

Because of the large size of the numerical model and taking into account the computer's computational power, the minimum particle size for this model is 0.3 m and the particle size ratio is 1.66, model gravity acceleration g, was set to 9.8 m/s^2. According to research by Yang (et al., 2006), when the ratio of the shortest edge to the particle size is greater than 80, the influence of the model size on the macro properties of the material can be neglected. In our model, the ratio of the shortest edge to the particle size is far greater than 80, therefore the choice of particle size is reasonable.

3.2. Physical model

The physical model is essentially a two dimensional model and the main similarity constants of the model are shown in the Table 3. The model is mainly composed of fine sand, calcite,

TABLE 3

Main constants of similar simulation experiment

Parameters	Value
Geometrical scale	1:100
Bulk density similarity ratio	1:1.67
Stress similarity ratio	1:167
Kinetic similarity constant	3.32×10^7
Time similarity ratio	1:7

gypsum, and water. The thicknesses and amounts of the different materials used to compose each layer are listed in Table 4. During the construction of the physical model, we attempted to faithfully produce a scaled version of the actual thickness of each coal or rock layer to ensure a smooth and uniform layering. Meanwhile, we added a layer of mica powder between each two rock layers – to make the model stratification clearer.

TABLE 4

Thicknesses and weight of material used in each layer of the physical model

Stratum number	Lithology	Thickness /cm	Gross dry weight/kg	Sand /kg	Calcium carbonate/kg	Gypsum /kg	Water /kg
1	Aeolian Sand	17	283.50	252.00	18.90	22.05	35.44
2	Siltstone	60	540.00	462.86	45.00	38.57	67.50
3	Medium Sandstone	3	31.50	25.20	2.36	1.89	3.94
4	Coal	5.91	54.00	46.29	4.50	2.31	6.75
5	Sandy Mudstone	2	18.00	15.00	0.90	2.10	3.00
6	Sandy Mudstone	33	297.00	254.57	19.80	21.21	37.13
7	Sandy Mudstone	4	40.50	33.75	3.24	4.73	6.75
8	Coal	7.25	61.20	52.46	5.25	2.62	7.65
9	Sandy Mudstone	7.84	75.60	64.80	6.62	5.40	9.45

4. Simulations

4.1. Numerical simulation

The simulation was designed to reproduce the sequence of phenomena that took place in the actual mine, so the first step was to simulate mining of the upper coal seam. The upper coal seam was mined in 10 m increments by reducing the velocity of model particles in that interval to zero. Then another 10 m was mined and this was repeated until the entire upper coal seam had been mined. After movement in the overlying strata stabilized, mining of the lower coal seam was begun. The lower coal seam face was advanced in 17 meters steps using the same procedure used for simulated mining of the upper coal seam.

In order to investigate the effect of mining the subjacent or underlying seam on fracture development in the overlying strata, a set of circles were delineated in the overlying strata after the upper coal seam had been mined (Fig. 1). These circles are used to calculate the permeability in the fractured areas. Then the fractured areas were divided according to their permeabilities. Permeability is calculated from Eq. (5), the Carman-Kozeny equation (Itasca, 2014; Bear, 1983):

$$K = B \times \frac{\varphi^3}{(1-\varphi)^2} \times d^2 \tag{5}$$

where K is absolute permeability, m^2; B is a geometric factor ranging from 0.003333 to 0.006667; φ is porosity; d is particle size, m. The value of variable d is based on the lithology of the measuring area, for the aeolian sand, d is $7.4e^{-5}$ m, and for the siltstone, it is $6.25e^{-5}$ m.

4.2. Physical simulation

The physical experiment was carried out in a manner similar to the numerical simulation. First, the upper coal seam was excavated in 10 cm increments. This is equivalent to advancing the working face of 10 m. The next 10 m excavation was carried out after the overlying strata had stabilized. The lower coal seam was mined 17 cm at a time using the same methods that were used to excavate the upper coal seam. During the experiment, a digital camera was used to record crack evolution.

5. Results and analysis

5.1. Model validation

The initial collapse of the roofs in the two models is shown in Fig. 2. It can be seen that when the working face in the upper coal seam has been advanced about 50 m, the first collapse of the roofs in the two models takes place. The first collapsing interval of coal face is 40-50 m, the periodic collapsing length is 12-17 m, which is in good agreement with the numerical simulation and similar experiment. Figure 3 shows collapse after mining of the upper coal seam has been completed. When the numerically simulated working face in the lower coal seam has advanced 68 m and the correlative lower seam working face in the physical experiment has advanced 85 m, the upper and lower goafs begin to join and form a composite goaf (Fig. 3). Figure 4 shows the planar, inclined fractures or fracture zones on the left and right sides of both models after mining

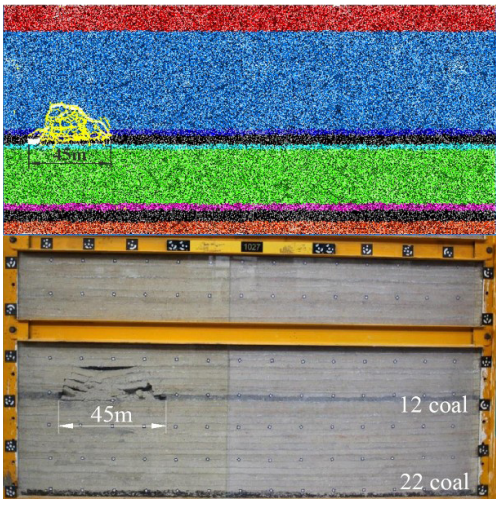

Fig. 2a. Initial collapse of upper coal seam roof. The upper part of the images were generated from the numerical model, the lower part are photographs of the physical model. The fractures in the images in the upper part are shown by the yellow lines

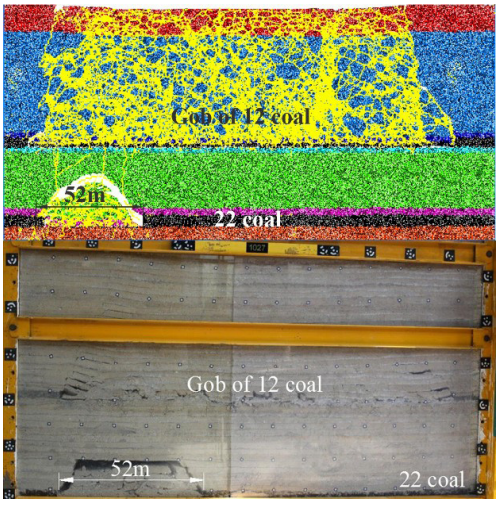

Fig. 2b. Initial collapse of lower coal seam roof. The upper part of the images were generated from the numerical model, the lower part are photographs of the physical model. The fractures in the images in the upper part are shown by the yellow lines

of the lower coal seam has been completed. Note that the inclined fractures produced by the two models dip at similar angles.

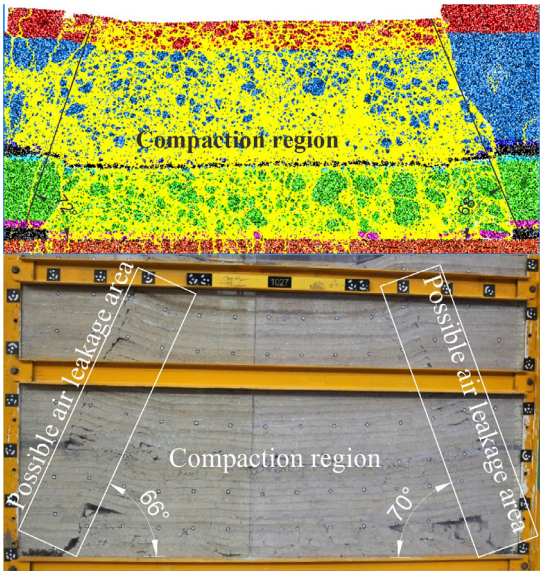

Fig. 3. The formation of a composite goaf after mining of the upper coal seam has been completed. The fractures above in the image are shown by the yellow lines

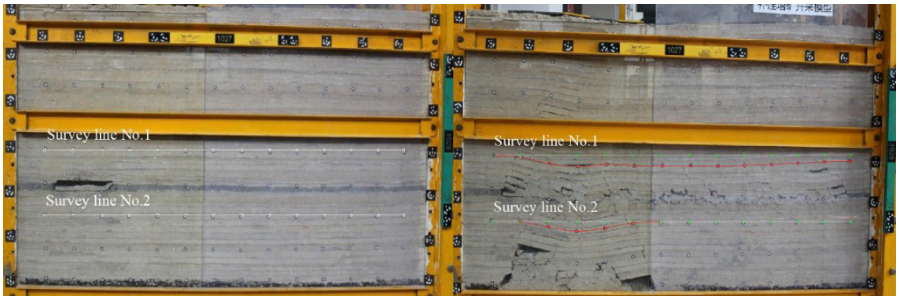

Fig. 4. The fractures after mining of the lower coal seam has been completed. The fractures above in the image are shown by the yellow lines

Comparing the subsidence of each point on the two survey lines when the coal seam started to be mined and the composite goaf was formed, as shown in Fig. 5 and Fig. 6, the maximum distance difference between the two model's survey line is only 1.42 m, and the trend of subsidence curve is similar, which shows that the similarity experiment and numerical calculation have good consistency.

Combined the similar experiment and numerical simulation, the characteristics of overburden rock collapse and the variation of mine pressure in working face are shown in Table 5. It is

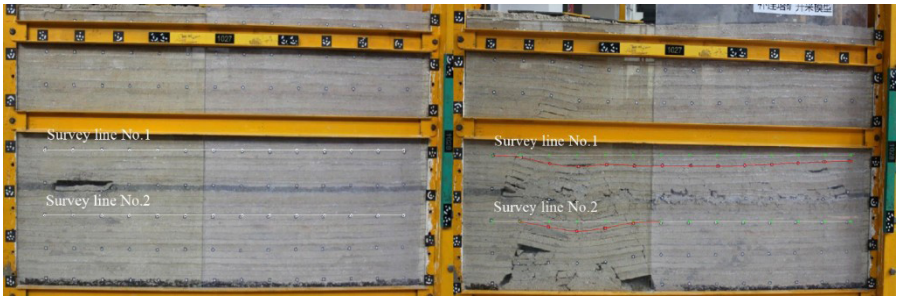

Fig. 5. The position of the survey lines

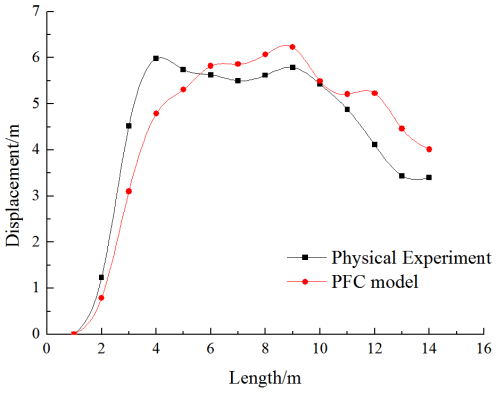

Fig. 6a. The subsidence of each point on the two survey lines. (Survey line No. 1)

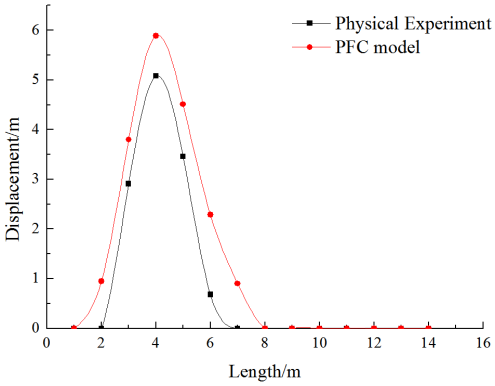

Fig. 6b. The subsidence of each point on the two survey lines. (Survey line No. 2)

found that the two methods show good consistency with the overlying formation of the overlying rock and the subsidence of the measured points, and the periodic pressure step is in good agreement with the actual period of the 22307 working face. So, the numerical simulation method in this paper can objectively reflect the collapse characteristics of the overlying rock in actual mining process.

TABLE 5

Comparison of weighting intervals demonstrated and fracture angles produced by the numerical simulation and the physical experiment

	Periodic weighting interval /m		**Strata fracture angle /°**		**Formed composite goaf /m**
	Upper coal seam	**Lower coal seam**	**Open-off cut**	**Stopping line**	
numerical simulation	14	15	72	68	68
similar experimental	15	15	66	70	85
Mining distance	12~17		—		—

5.2. Effect of multi-seam mining on fracture development

In order to quantitatively analyze the differences in fracture developed in the overlying strata an underlying coal seam has been mined, we used Eq. (5) to evaluate the permeability of the eight rows of measuring circles shown in Fig. 1. The results show that after mining the upper coal seam, the permeability in first and second row is about 10^{-10}, in third row to fifth row is about 10^{-11}, in the sixth through eighth rows is about 10^{-12}. To analyze the fractured areas, group the first and second row, the third to fifth rows were combined as a second group, and the six to eight rows were combined into a third group. These groups are labeled A, B, and C (Fig. 7). Additionally, each group was divided into sub-vertical sections each section being about 50 meters wide (the areas labeled 1-5 plus sections D and E, Fig. 7). All of the fracture areas are shown in Fig. 7; the yellow lines indicate the fractures.

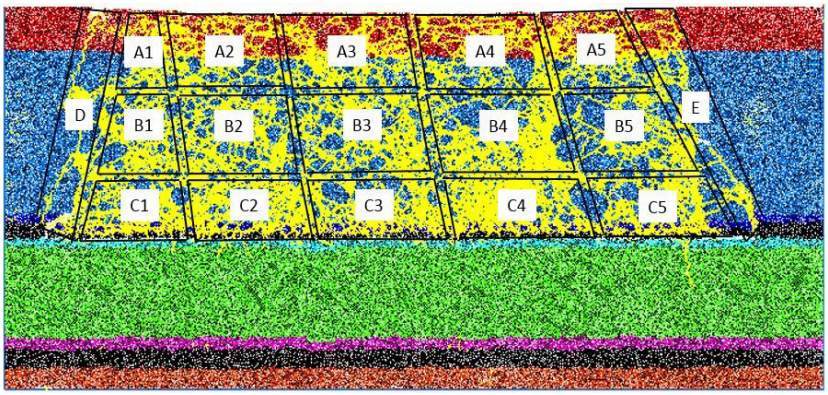

Fig. 7. The overlying strata divided into fracture areas. The strata have been divided into fracture groups (areas labeled A-C) and fracture sections (areas labeled 1–5 plus D and E). The fractures are shown by the yellow lines

Using the method propose by Hiroyuki (Shimizu et al., 2011), we have counted the number of fractures in each area before and after the mining of the lower coal seam and compared the number of fractures in the different groups and sections. The results are shown in Fig. 8.

It can be seen from Fig. 8 that the number of fractures in each area increases after the lower coal seam is mined, especially the number of fractures in the open-off cut and stopping line sections (the regions labeled D and E). The number of fractures in those two areas increases the most. Figure 8(a) shows that mining the lower coal seam has a notable influence on fracture development in the area adjacent to the upper coal seam goaf (group C). Figure 8(b) shows that mining the lower coal seam also has a significant influence on new fracture development in the open-off cut and stopping line areas of the upper coal seam. However, during mining of the upper coal seam, fractures in the overlying strata above the goaf developed more fully; during lower coal seam mining, the growth rate of the number of fractures was low (as shown in sections 2, 3, and 4).

In order to analyze the variations in the number of fractures in each section during working face advance, the number of fractures in sections 1, 2, 3, 4, 5, D, and E were tabulated for each

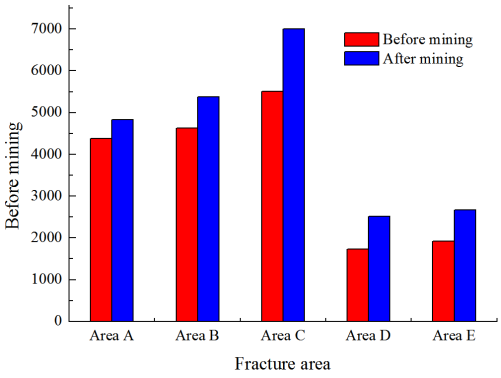

Fig. 8a. Number of fractures in horizontal groups

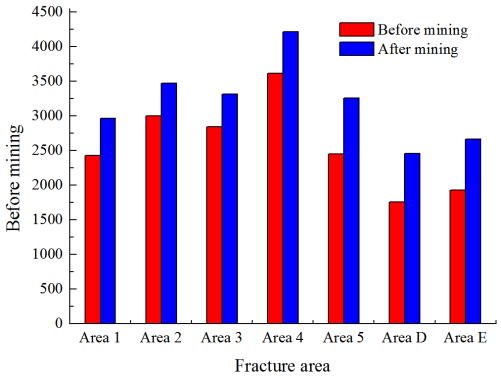

Fig. 8b. Number of fractures in vertical sections

advance of the lower coal seam working face. The results are shown in Fig. 9. It can be seen that during mining of the lower coal seam, the number of fractures in each section of the overlying strata show a „stability-rapid increase-stability“ pattern but the pattern is clearly different in each of the different sections. For example, in section 3, fracture numbers increases rapidly when working face advances to about 120 m but the rate of increase begins to slow down when working face advances to about 200 m. For the D and E sections, fracture numbers in D increases rapidly when working face advances to about 17 m and slows down when the working face reaches 68 m. However, fracture numbers in section E do not change when working face begins to advance and only increases rapidly when the working face advances to 204 m.

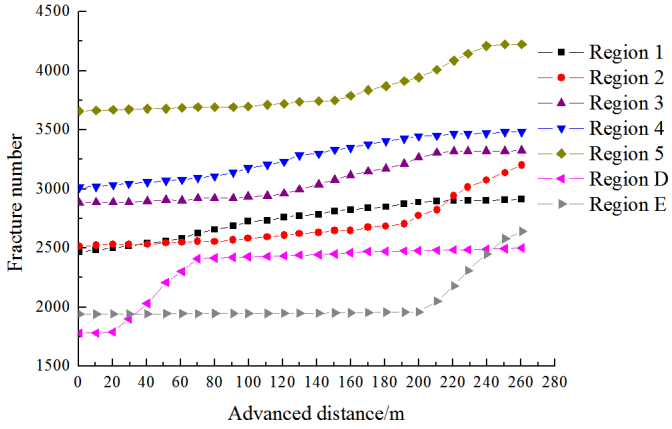

Fig. 9. Number of fractures in the seven sections shown in Fig. 7 for each 17 m working face advance during lower coal seam mining. The number of fractures for sections 1 through 5, sections D and E is shown in the graph

5.3. Effects of multi-seam mining on permeability in the overlying strata

After the upper coal seam had been mined out and the overlying strata had stabilized, a number of measuring circles were delineated in the overlying strata to determine their porosity. In order to improve accuracy, four measuring circles were defined in the same area and the average value was calculated and used to represent the average porosity of that area.

The change in permeability for areas A3, B3, C3, D, and E (Fig. 7) during advance of the lower coal seam working face is shown in Fig. 10. It can be seen that during lower coal seam mining, permeability in each fracture area in the upper goaf also presents the „stability-rapid increase-stability" pattern. Taking area A3 as an example, when the working face advances to about 68 m, permeability in area A3 increases rapidly and the rate of permeability increase remains essentially constant until the working face advances to about 170 m. The horizontal distance between the left boundary of the A3 area and the open-off cut above the lower coal seam is about 75 m and the horizontal distance between the right A3 boundary and open-off cut is about 155 m. Simple calculations show that the influence of working face advance on the A3 area porosity takes place about 7 m ahead of the working face and continues until the face has advanced about 15 m beyond the A3 area. Similar precursory and lag behavior is evident in the porosity graphs for the other areas.

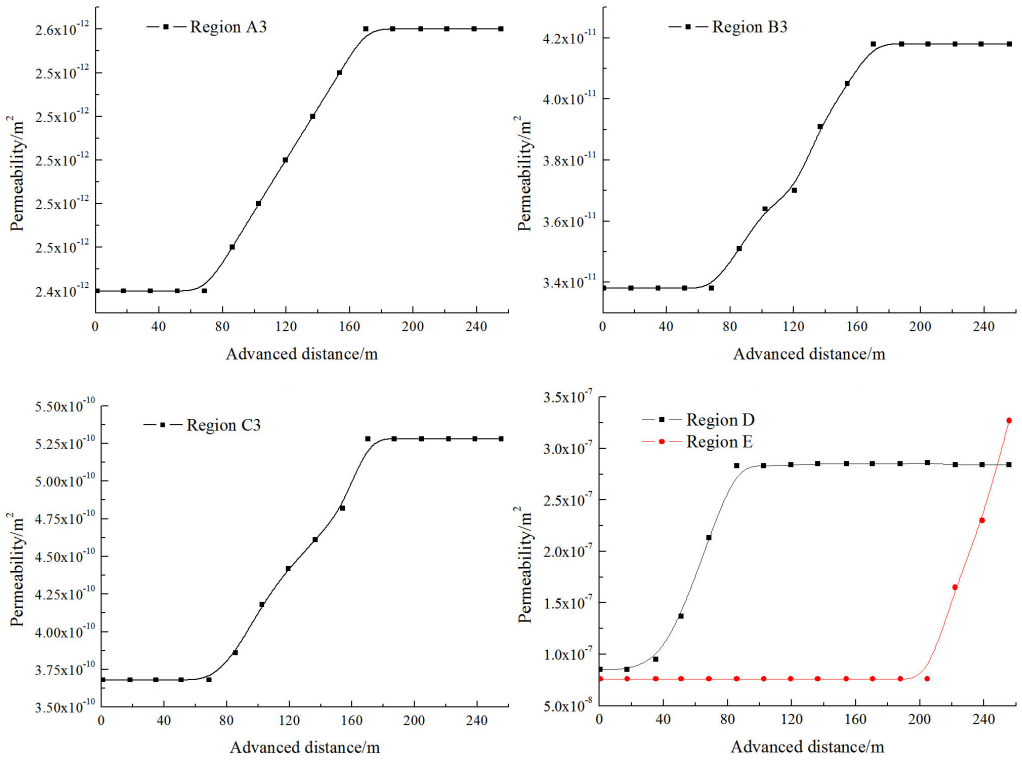

Fig. 10. The changes in permeability in the A3, B3, C3, D, and E areas vs. lower coal mining face advance

The changes in permeability for each group and for areas D and E before and after lower coal seam mining were also calculated. The results are shown in Fig. 11. It can be seen that the permeability in each area increases to different degrees after lower coal seam mining and the permeabilities in the open-off cut and the stopping line areas, areas D and E, have the largest increase whereas the permeability increases in the overlying strata above the goaf are relatively small. The reason is that during working face advance, there are large fractures that do not close in the open-off cut and stopping line areas. Because of collapse, the fractures in the separate layers are gradually compacted to form a structure above the middle of the goaf with a dense center and looser margins; this structure is called the „O-circle“ (Qian & Xu, 1998). Because of the “O circle,” the permeability in different area of the boundary area around the goaf varies greatly but the change in permeability in the central area is small.

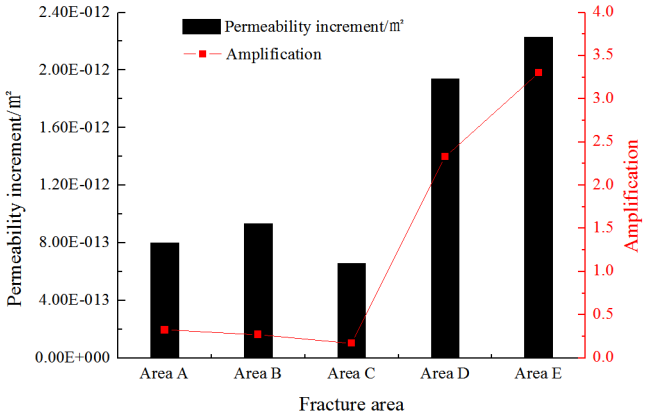

Fig. 11. The increasing range of permeability in different areas in the overlying strata after lower coal seam mining

5.4. Effects of multi-seam mining on air leakage

Figure 12 shows how large air leakage fractures in the goaf change after the lower coal seam is mined. It can be seen from the figure that because the overlying strata collapse, large air leakage fractures at the open-off cut of the upper coal seam are further developed and the width of air leakage fractures near the stopping line is increased. On both sides of the model, especially near the surface, the fracture widths increase and the width of the largest fracture is more than 1 m. Combined with the changes in permeability in the area, the model shows that the open-off cut and stopping line areas are the main conduits for air leaking into the

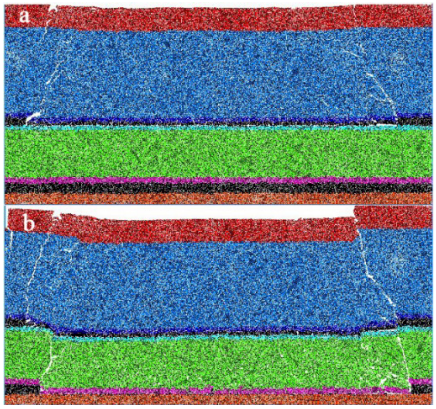

Fig. 12. The large air leakage fractures change after the lower coal seam is mined. Fractures are shown as white lines

compound goaf. These are the important areas in which air movement should be minimized to prevent spontaneous combustion in the goaf.

6. Conclusions

(1) When shallow and closely spaced coal seams are mined, mining the lower coal seam has a serious effect on the upper goaf. Mining the lower seam results in the generation of secondary ruptures in the overlying coal and rock, further development of large air leakage fractures at the open-off cut of the upper coal seam, significant increases in width of air leakage fractures near the stopping line, and the formation of a compound goaf.

(2) During lower coal seam mining, the fractures redevelopment in each area above the lower coal seam has different patterns but all the patterns have the same form, and the number of fractures and the permeability of areas above the seam show a pattern of „stability-rapid increase-stability."

(3) After shallow and closely spaced coal seams are mined, the permeability increment of each fracture zone is Area A:0.8E-12 m^2; Area B:0.932E-12 m^2; Area C:0.659E-12 m^2; Area D:1.99E-12 m^2; Area E:2.5E-12 m^2, the variation range of overburden permeability in the open cut and stop line area (area D and area E) is much larger than that in other areas, and the main air leakage passage in compound goaf can be formed in this two areas. So, region D and region E are the key areas for preventing coal spontaneous combustion in goaf by blocking leakage and controlling measures.

Acknowledgements

We are grateful for the Natural Science Foundation of China (grant no. 51774276) and funding from the Priority Academic Program Development of the Jiangsu Higher Education Institutions.

References

Bear J., 1983. *Dynamics of fluids in porous media.* Beijing:China Architecture and Building Press, 1-345.

Cheng Zhiheng, Qi Qingxin, Li Hongyan et al., 2016. *Evolution of the superimposed mining induced stress-fissure field under extracting of close distance coal seam group.* Journal of China Coal Society **41** (2), 367-375.

Cheng Zhi-Heng, Qi Qing-Xin, Li Hong-Yan, Zhang Lang, Liu Xiao-Gang, 2017. *Evolution of the superimposed mining induced stress-fissure field underextracting of close distance coal seam group.* Journal of Safety Science and Technology **27** (6), 133-138.

Chu Tingxiang, Yu Minggao, Yang Shengqiang, JiaHailin, 2010. *Air leaking induced by well developed coal fracturesand prevention of spontaneous combustion in goaf.* Journal of Mining and Safety Engineering **27** (1), 87-93.

Cymbarerich M., 1957. *Mine support*. BeiJing: China Coal Industry Publishing House (in Chinese).

Fan Gang-Wei, Zhang Dons-Sheng, Ma Li-Qiang, 2011. *Overburden movement and fracture distribution induced by longwall of the shallow coal seam in the Shendong mining coalfield.* Journal of China University of Mining and Technology **40** (2), 196-201.

Guo H., Yuan L., Shen B., Qu Q., Xue J., 2012. *Mining-induced strata stress changes, fractures and gas flow dynamics in multi-seam longwall mining.* International Journal of Rock Mechanics & Mining Sciences **54** (3), 129-139.

Holla L., 2012. *Some Aspects of Strata Movement relating to Mining under Water Bodies in J'Tew South Wales, Australia.* International Mine Water Association 2012.

Holla L., Buizen M., 1991. *The ground movement, strata fracturing and changes in permeability due to deep longwall mining*. International Journal of Rock Mechanics & Mining Science & Geomechanics Abstracts **28** (2-3), 207-217.

Hu Chenglin, 2014. *Law of Overburden Fracture Evolution in Shallow Buried Close Distance Coal SeamUnder Repeated Mining* [D]. China University of Mining and Technology, Xuzhou.

Itasca Consulting Group Inc, 2014. PFC2D/3D (Particle Flow Code in2/3 Dimensions),Version 5.0. Minneapolis, Itasca Consulting Group, 2014.

Jiang Fuxing, Jiang Guoan, Tan Yunliang, 2002. *Discussion on Mining Method of Shallow Buried Hard Roof Thick Seam in India.* Mine Pressure and Roof Management (1), 57-59 (in Chinese).

Jin Zhiyuan, 2015. *Development Laws and Control of Overlying Strata Water Flowing Fractures in Repeated Disturbance Zone of Shallowly-buried Short-distance Coal Seams* [D]. China University of Mining and Technology, Xuzhou.

Li Tao, Li Wenping, Chang Jinyuan, Du Pingping, Gao Ying, 2011. *Permeability Features of Water-Resistant Clay Layer in NorthernShaanxi Province While Shallowly Buried Coal Mining*. Journal of Mining and Safety Engineering **28**, 127-131.

Ma Haifeng, Cheng Zhiheng, Liu Wei, 2017. *Evolution characteristics of mining stress and overlying strata displacementfield under superimposed mining in close distance coal seam group.* Journal of Safety Science and Technology **13** (5), 28-33.

Ma L., Cao, Liu Q., Zhou T., 2013. *Simulation study on water-preserved mining in multi-excavation disturbed zone in close-distance seams.* Environmental Engineering & Management Journal **12** (9), 1849-1853.

Ma L., Jin Z., Liang J., Sun H., Zhang D., Li P.. 2015. *Simulation of water resource loss in short-distance coal seams disturbed by repeated mining.* Environmental Earth Sciences **74** (7), 5653-5662.

Qian Minggao, Xu Jialin, 1998. *Study on the "o-shape" circle distribution characteristics of mining- induced fractures in the overlaying strata.* Journal of China Coal Society **23** (5), 466-469.

Shimizu H., Murata S., Ishida T., 2011. T*he distinct element analysis for hydraulic fracturing in hard rock considering fluid viscosity and particle size distribution.* International Journal of Rock Mechanics & Mining Sciences **48** (5), 712-727.

Singh R.P., Yadav R.N., 1995. *Subsidence due to coal mining in India.* International Journal of Rock Mechanics & Mining Sciences & Geomechanics Abstracts (7), 331A.

TaoWang, Weibo Zhou, Jinhu Chen, XiongXiao, YangLi, Xianyu Zhao, 2014. *Simulation of hydraulic fracturing using particle flow method and application in a coal mine.* International Journal of Coal Geology **121** (Complete), 1-13.

Tianrang J., Zimin Z., Chunan T., Yongjun Z., 2013. *Numerical Simulation of Stress-Relief Effects of Protective Layer Extraction.* Archives of Mining Sciences **58**, 521-540.

Tu H.S., Zhang C., Zhang L., Zhang X.G., 2017. *Characteristics of the Roof Behaviors and Mine Pressure Manifestations During the Mining of Steep Coal Seam.* Archives of Mining Sciences **62**.

Wang Fangtian, 2012. *Overlying Strata Movement Laws and Ground Control of the Longwall Face Mining in a Shallow Depth Seam in Proximity beneath a Room Mining Goaf* [D]. China University of Mining and Technology, Xuzhou.

Wen Hu, Yu Zhijin, Zhai Xiaowei, Liu Leizheng, Zhao Jingyu, 2015. *Crack Development and Interconnected Characteristics of Closely Spaced Shallow Coal Seams Under Overlapping Mining.* Safety in Coal Mines **46** (12), 46-49.

Xue Dongjie, Zhou Hongwei, Ren Weiguang, Zhang Bo-Fu, Liu Ya-Qun, Zhao Yu-Feng, 2015. *Stepped shearing-induced failure mechanism and cracks propagation of overlying thin bedrocks in shallow deep coal seams mining*. Journal of China Coal Society **40** (8), 1746-1752.

Yang B., Jiao Y., Lei S., 2006. *A study on the effects of microparameters on macroproperties for specimens created by bonded particles.* Engineering Computations **23** (6), 607-631.

Zhang Xiaomei, 2012. *Gas Explosion Risk Analysis On Face of Closing-Fire-Districtin Coal Mine.* Xi'an:Xi'an University of Science and Technology.

Zhao Tuanzhi, Li Wenping, Li Xiaoqin, Sun Ruhua, Zheng Zhijun, 2009.*Numerical simulation on dynamic changes of stress andover burden bed separation concerned with superimposed mining*. Journal of Mining and Safety Engineering **26** (1), 118-122.

Zhu Weibing, 2010. *Study on the Instability Mechanism of Key Strata Structure in Repeat Mining of Shallow Close Distance Seams* [D]. China University of Mining and Technology, Xuzhou.